Inorganica Chimica Acta 363 (2010) 2001–2008

Contents lists available at ScienceDirect

Inorganica Chimica Acta

journal homepage: www.elsevier.com/locate/ica

Unusual ligand design: A platinum(II) mediated [2+2] photocycloaddition followed by a nickel(II) induced methoxyactivation

Markus Fessler [a], Georg Czermak [a], Sylvia Eller [a], Barbara Trettenbrein [a], Stephan Haringer [a], Werner Oberhauser [b], Peter Brüggeller [a,*]

[a] Institut für Allgemeine, Anorganische und Theoretische Chemie der Universität Innsbruck, Innrain 52a, 6020 Innsbruck, Austria
[b] Istituto di Chimica dei Composti Organometallici (ICCOM-CNR), Area di Ricerca CNR di Firenze, via Madonna del Piano 10, 50019 Sesto Fiorentino, Italy

ARTICLE INFO

Article history:
Received 18 December 2008
Accepted 8 March 2009
Available online 16 March 2009

Dedicated to Prof. Umberto Belluco

Keywords:
Nickel(II) complexes
Tetraphosphane
Methoxy-group cleavage
X-ray crystallography
Phosphanophenolate
P-chirality

ABSTRACT

The novel dimer of the composition $[Pt_2Cl_4(\mu\text{-}(\kappa P^1{:}\kappa P^2\text{-}o\text{-MeO-}trans\text{-dppen}))_2]$ (**1**) (*o*-MeO-*trans*-dppen = 1,2-(bis(*o*-methoxyphenyl)phosphanyl)ethylene) has been prepared and characterized by a single crystal X-ray structure analysis, NMR spectroscopy, mass spectrometry and elemental analysis. This latter compound undergoes a [2+2] photocycloaddition reaction yielding the tetraphosphane all-*trans*-1,2,3,4-tetrakis(di(*o*-methoxyphenyl)phosphanyl)cyclobutane (*o*-MeO-dppcb). The X-ray structure of the dimeric Ni(II) complex that contains the latter ligand, of the formula $[Ni_2Cl_4(\mu\text{-}(\kappa P^1{:}\kappa P^2{:}\kappa P^3{:}\kappa P^4\text{-}o\text{-MeO-dppcb}))]$ (**2**) reveals that the apical coordination sites of both square pyramidal Ni(II) coordination spheres are occupied by methoxy-oxygen atoms of the ligand. As a consequence, this dimeric Ni(II) complex **2** is prone to a thermally induced regio- and diastereoselective metal-assisted methoxy-group cleavage. The stepwise formed new mono- and bis-phenolate complexes $[Ni_2Cl_3(\mu\text{-}(\kappa O^1,\kappa P^1{:}\kappa P^2{:}\kappa P^3{:}\kappa P^4\text{-}o\text{-MeO-}O\text{-dppcb}))]$ (**3**) and $[Ni_2Cl_2(\mu\text{-}(\kappa O^1,\kappa P^1{:}\kappa P^2{:}\kappa O^2,\kappa P^3{:}\kappa P^4\text{-}o\text{-MeO-}O,O'\text{-dppcb}))]$ (**4**), respectively, contain the novel chiral tetraphosphane ligands all-*trans*-1,2,3-tris((di-*o*-methoxyphenyl)phosphano)-4-((*o*-methoxy-phenyl)(*o*-phenolate)phosphano)cyclobutane (*o*-MeO-*O*-dppcb) and all-*trans*-1,2-bis((di-*o*-methoxyphenyl)phosphano)-3,4-bis((*o*-methoxyphenyl)(*o*-phenolate)phosphano)cyclobutane (*o*-MeO-*O,O′*-dppcb). Compounds **3** and **4** have been synthesized independently and are also fully characterized by both single crystal X-ray structure analyses, NMR spectroscopy, mass spectrometry and elemental analyses. The conversion of **2** into **3** and then further into **4** has been followed by a variable-temperature $^{31}P\{^1H\}$ NMR experiment with compound **2** in DMF-d^7, revealing that the cleavage of the second methoxy group is kinetically disfavoured. This is in agreement with the X-ray structure analysis of **3**, indicating the lack of any methoxy-oxygen atom coordination that could easily induce a further methoxy-group cleavage. *o*-MeO-*O*-dppcb and *o*-MeO-*O,O′*-dppcb are rare P-stereogenic tetraphosphine ligands and contribute to the synthetic field of new κ^3-*P,P,O*-coordinating phosphanylphenolate ligands that are believed to be important for the SHOP process (SHOP, Shell Higher Olefin Process).

1. Introduction

Catalytic systems, that are obtained by the combination of Ni(II) with a κ^2-*P,O*-chelating ligand were found to be very efficient for the SHOP process (SHOP, Shell Higher Olefin Process) [1].

Among the κ^2-*P,O*-chelating ligands used for this latter important industrial process, phosphanoenolates are particular attractive, since the negatively charged oxygen atom efficiently coordinates to the metal center, stabilizing various metallorganic species that take part in the catalytic cycle of the α-olefin oligomerization reaction [1a]. In this context, a complex with the general formula $[Ni(\kappa^2\text{-}P,O\text{-L})Ph(PPh_3)]$ (L = 2-phenyl-diphenylphosphanoenolate) (Scheme 1, a) has been synthesized and successfully applied by Keim et al. for the oligomerization of ethylene [1b].

Since then, a great deal of synthetic protocols appeared in the literature aimed at synthesizing phosphanoenolates and 2-phosphanophenolates. Among them are of particular synthetic importance the reaction of 2-lithio-lithiumphenolates with chlorophosphanes [2], the metallation of 2-bromo-phenylphosphanites with sodium [3] and the *ortho*-metalation of phenylmethoxymethylethers and the subsequent reaction with chlorophosphanes [4]. Furthermore, also metal-assisted synthetic methods are known like nickel catalyzed arylations of triarylphosphanes and subsequent cleavage of

* Corresponding author. Fax: +43 512 5072934.
E-mail address: Peter.Brueggeller@uibk.ac.at (P. Brüggeller).

0020-1693/$ - see front matter © 2009 Elsevier B.V. All rights reserved.
doi:10.1016/j.ica.2009.03.009

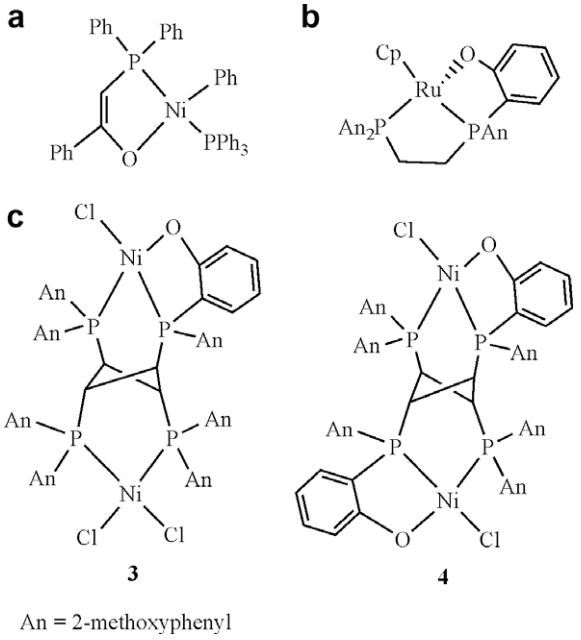

Scheme 1.

an aryl group [5,6]. The reaction of *o*-benzochinone-2-ylidene-triphenylphosphorane with [Ni(η^4-COD)$_2$] (COD = 1,5-cyclooctadiene) [7] also resulted to be one of the most applied synthesis paths.

In the past decade P-stereogenic diphosphane ligands have played a pivotal role in the creation of a strictly defined asymmetric environment around the metal center [8]. In this context, chiral phosphanylphenolate ligands, capable of coordinating metals in a κ^3-*P,P,O*-mode, are much less studied compared to κ^2-*P,O*-coordinating phosphanylphenolates. In fact, only (2-((2-bis(*o*-methoxyphenyl)phosphano)ethyl)(*o*-methoxyphenyl)phosphano)phenolate [9] that coordinates in a κ^3-*P,P,O*-fashion to Ru(II) is known up to now (Scheme 1, b). The simultaneous coordination of two soft donor atoms such as phosphorus and a negatively charged hard phenolate oxygen atom may give rise to a rich coordination chemistry of this kind of ligands endowing the metal center with unique electronic properties.

In order to contribute in this field of synthetic chemistry, especially of new κ^3-*P,P,O*-coordinating phosphanophenolate ligands, we report the synthesis of the two novel bridging phosphanylphenolate ligands all-*trans*-1,2,3- tris((di-*o*-methoxyphenyl)phosphano)-4-((*o*-methoxyphenyl)(*o*-phenolate)phosphano) cyclobutane (*o*-MeO-*O*-dppcb) and all-*trans*-1,2-bis((di-*o*-methoxyphenyl)phosphano)-3,4-bis((*o*-methoxyphenyl)(*o*-phenolate)phosphano)cyclobutane (*o*-MeO-*O,O′*-dppcb) coordinated to Ni(II). Thus, these ligands yield [Ni_2Cl_3(μ-(κO^1,κP^1:κP^2:κP^3:κP^4-*o*-MeO-*O*-dppcb))] (**3**) and [Ni_2Cl_2(μ-(κO^1,κP^1:κP^2:κO^2,κP^3:κP^4-*o*-MeO-*O,O′*-dppcb))] (**4**), respectively (Scheme 1, c). The key steps for the synthesis of both latter complexes are an intramolecular [2+2] photocycloaddition reaction of the new binuclear complex [Pt_2Cl_4(μ-(κP^1:κP^2-*o*-MeO-*trans*-dppen))$_2$] (**1**) (*o*-MeO-*trans*-dppen = 1,2-(bis(*o*-methoxyphenyl) phosphanyl)ethylene), that yields all-*trans*-1,2,3,4-tetrakis(di(*o*-methoxyphenyl)phosphanyl) cyclobutane (*o*-MeO-dppcb), upon a cyanolysis reaction of the photochemically obtained Pt-intermediate and a thermally induced methoxy-group cleavage in the dimeric Ni(II) complex of the latter ligand of the formula [Ni_2Cl_4(μ-(κP^1:κP^2:κP^3:κP^4-*o*-MeO-dppcb))] (**2**). This reaction represents a unique regio- and diastereoselective metal-assisted methoxy-group cleavage. The single crystal X-ray structures of **1** · 4CH_2Cl_2, **2** · 2.5$C_2H_4Cl_2$ · H_2O, **3** · 3DMF and **4** · 2CH_3CN are reported and discussed.

2. Experimental

2.1. General procedures, methods and materials

All syntheses have been performed under a dry argon atmosphere applying standard Schlenk techniques. Solvents have been dried over suitable activated molecular sieves and deaerated prior to use. Bis(*o*-methoxyphenyl)phosphane [10], compound **2** [11], *o*-MeO-*trans*-dppen [11], and *o*-MeO-dppcb [11] were synthesized according to literature methods, while all other reagents were used as purchased from Aldrich or Strem. Deuterated solvents for routine NMR measurements were used as purchased from EuroIsotop. ^{1}H, ^{13}C{^{1}H}, and ^{31}P{^{1}H} NMR spectra were obtained on a Bruker Avance DPX 300 spectrometer, measuring at 300.13, 75.48, and 121.50 MHz, respectively. Chemical shifts (δ) are reported in ppm relative to TMS (^{1}H and ^{13}C{^{1}H} NMR) or 85% H_3PO_4 (^{31}P{^{1}H} NMR). Elemental analyses were performed using a Perkin–Elmer Model 2400 elemental analyser. FAB mass spectrometry measurements have been carried out on a Finnigan MAT-95 spectrometer, using 3-nitrobenzylalcohol (NOBA) as matrix. The ^{31}P{^{1}H} NMR spectrum of compound **4** has been simulated using the INSIM-GUI V 1.0 program [12].

2.2. Synthesis of [Pt_2Cl_4(μ-(κP^1:κP^2-*o*-MeO-*trans*-dppen))$_2$] (**1**)

[$PtCl_2$(η^4-COD)] (3.74 g, 10.0 mmol) was added to a deaerated solution of *o*-MeO-*trans*-dppen (5.16 g, 10.0 mmol) in CH_2Cl_2 (200 ml) at room temperature. The reaction mixture was allowed to stir overnight. The solid formed was then separated by filtration, washed with CH_2Cl_2 (3 × 50 ml) and dried under vacuum. Yield 7.22 g (92.2%). Mp >350 °C. *Anal.* Calc. for $C_{60}H_{60}Cl_4O_8P_4Pt_2$ (1564.92): C, 46.05; H, 3.86. Found: C, 45.97; H, 3.93%. ^{1}H NMR (CD_2Cl_2, 25 °C): δ 2.68–2.90 (br m, 12H, O*CH*$_3$), 3.63–3.78 (br m, 12H, O*CH*$_3$), 5.01 (m, 2H, *CH*=*CH*), 5.60 (m, 2H, *CH*=*CH*), 6.98–7.61 (br m, 32H, Ar–*H*). ^{31}P{^{1}H} NMR (CD_2Cl_2, 25 °C): δ −5.9 (s, $^1J_{PtP}$ = 3640.0 Hz). MS (FAB+) *m*/*z*: 1529.71 (M^++H).

2.3. Synthesis of [Ni_2Cl_3(μ-(κO^1,κP^1:κP^2:κP^3:κP^4-*o*-MeO-*O*-dppcb))] (**3**)

A deaerated solution of compound **2** (40.0 mg, 0.031 mmol) in DMF (15.0 mL) was placed into a Schlenk tube. The red solution was heated at 80 °C for 1.5 h under nitrogen. The red solution was then cooled to room temperature and the solvent removed by means of a vacuum pump. The crude product was suspended in diethyl ether (25 ml), stirred for 10 min, separated by filtration and dried under vacuum. Yield 23.8 mg (61.8%). Mp = 174 °C dec. *Anal.* Calc. for $C_{59}H_{57}Cl_3Ni_2O_8P_4$ (1241.705): C, 57.07; H, 4.63. Found: C, 56.95; H, 4.49%. ^{1}H NMR (CD_2Cl_2, 25 °C): δ 2.60–3.62 (br m, 21H, O*CH*$_3$), 4.33 (br s, 4H, P*CH*), 6.20–8.20 (m, 30H, Ar–*H*), 9.60 (br s, 1H, *o*-Ar–*H*), 10.82 (br s, 1H, *o*-Ar–*H*). ^{31}P{^{1}H} NMR (CD_2Cl_2, 25 °C): δ 9.43 (br s), 21.80 (br s), 29.25 (br s), 36.70 (br s). MS (FAB+) *m*/*z*: 1205.5 (M^+−Cl).

2.4. Synthesis of [Ni_2Cl_2(μ-(κO^1,κP^1:κP^2:κO^2,κP^3:κP^4-*o*-MeO-*O,O′*-dppcb)] (**4**)

A deaerated solution of compound **3** (35.0 mg, 0.028 mmol) in DMF (10.0 ml) was placed into a Schlenk tube under nitrogen. The clear red solution was heated at 100 °C for 1.5 h. Afterwards the solution was cooled to room temperature, followed by the evaporation of the solvent to dryness by means of a vacuum pump. The obtained red-brown powder was suspended in diethyl ether (20 ml) and stirred for 10 min. The solid product was separated by filtration and dried under vacuum. Yield 35.4 mg (95.9%). Mp >350 °C. *Anal.* Calc. for $C_{58}H_{54}Cl_2Ni_2O_8P_4$ (1191.22): C, 58.48; H, 4.57. Found: C, 58.33; H, 4.64%. ^{1}H NMR (CD_2Cl_2, 25 °C): δ 2.41

(d, $^2J_{PH}$ = 14 Hz, 2H, PC*H*), 2.80 (s, 3H, OCH_3), 2.89 (s, 3H, OCH_3), 3.06 (s, 6H, OCH_3), 3.39 (s, 6H, OCH_3), 4.58 (br d, $^2J_{PH}$ = 12 Hz, 2H, PC*H*), 6.3–7.7 (br m, 30H, Ar–*H*), 9.26 (br s, 1H, *o*-Ar–*H*), 9.57 (dd, $^3J_{PH}$ = 8 Hz, $^3J_{HH}$ = 8 Hz, 1H, *o*-Ar–*H*). ^{13}C{^{1}H} NMR (CD_2Cl_2, 25 °C): δ 31.55 (d, $^1J_{PC}$ = 28 Hz, P*C*H), 38.65 (d, $^1J_{PC}$ = 22 Hz, P*C*H), 54.22 (s, O*C*H_3), 55.24 (s, O*C*H_3), 110.32–142.66 (s, Ar–*C*), 158.61 (s, *C*–OCH$_3$), 159.87 (s, *C*–OCH$_3$), 175.23 (d, $^2J_{PC}$ = 20 Hz, Ar–*C*–O). ^{31}P{^{1}H} NMR (CD_2Cl_2, 25 °C): δ 22.70 (dd, $^2J_{PP}$ = 83 Hz, $^3J_{PP}$ = 29 Hz, $P_{achiral}$), 39.37 (br s, P_{chiral}). MS (FAB+) *m*/*z*: 1157.2 (M^+−Cl).

2.5. Variable-temperature NMR study of **2** in DMF-d^7

Compound **2** (6.0 mg, 0.005 mmol) was dissolved in deaerated DMF-d^7 (1.5 ml) and the obtained red solution was transferred into a 5 mm NMR tube under nitrogen and sealed. The NMR tube was then transferred into a NMR probe at room temperature, followed by the acquisition of a ^{31}P{^{1}H} NMR spectrum. Then the NMR probe was heated to 40 °C for half an hour, followed by the acquisition of a ^{31}P{^{1}H} NMR spectrum. Afterwards the NMR probe was cooled to room temperature and a ^{31}P{^{1}H} NMR spectrum at the latter temperature was acquired. This heating and cooling cycle was repeated until a temperature of 80 °C was reached, increasing the temperature from cycle to cycle in 10 °C steps. Once the conversion of **2** into **3** was completed, the NMR probe was heated to 100 °C and ^{31}P{^{1}H} NMR spectra were acquired at the latter temperature in time intervals of half an hour. As soon as no further changes of the ^{31}P{^{1}H} NMR peak intensities were observed and hence the conversion of **3** into **4** was completed, the NMR probe was cooled to room temperature followed by the acquisition of a final ^{31}P{^{1}H} NMR spectrum.

2.6. X-ray crystal structure determination

Single crystals of **1** · 4CH_2Cl_2 suitable for an X-ray diffraction study, that easily released the solvent molecules at room temperature within seconds, were obtained retrosynthetically via a liquid–liquid diffusion of deaerated CH_2Cl_2 solutions of [$PtCl_2$(η^4-COD)] and *trans*-*o*-MeO-dppen, respectively, into each other at room temperature. Single crystals of **2** · 2.5$C_2H_4Cl_2$ · H_2O, **3** · 3DMF and **4** · 4CH_3CN suitable for X-ray structure analyses were obtained by the evaporation of the corresponding $C_2H_4Cl_2$, DMF and CH_3CN solutions of **2**, **3** and **4** at room temperature. Crystallographic data and structure refinement details for all four compounds are summarized in Table 1. Diffraction data were collected on a Nonius Kappa CCD diffractometer using φ–ω-scans and graphite-monochromated Mo Kα radiation (λ = 0.71073 Å). Cell refinement, data reduction, and the empirical absorption correction were done by the DENZO and SCALEPACK programs [13]. All structure determination calculations were performed using SHELXTL NT V6.1 including SHELXS-97 and SHELXL-97 [14]. Final refinements on F^2 were carried out applying anisotropic thermal parameters for all non-hydrogen atoms, while all hydrogen atoms were included in the refinement using a riding model with isotropic *U*-values depending on the U_{eq} of the adjacent carbon atoms. The hydrogen atoms on O(9) of the water solvent molecule in structure **2**, on C(18), C(19) and C(20) of one DMF solvent molecule in structure **3**, and on C(9) of one MeCN solvent molecule in structure **4** have been omitted due to substantial disorder in these solvent molecules.

3. Results and discussion

3.1. Synthesis and crystal structure of [Pt_2Cl_4(μ-(κP^1:κP^2-*o*-MeO-*trans*-dppen))$_2$] (**1**)

The synthesis of *o*-MeO-dppcb has been achieved following the synthetic protocol as shown in Scheme 2. Although basic information about the synthesis of the latter ligand has already been reported [11], no explanation of the observed all-*trans*-

Table 1
Crystallographic data and structure refinement details for compounds **1** · 4CH_2Cl_2, **2** · 2.5$C_2H_4Cl_2$ · H_2O, **3** · 3DMF and **4** · 4CH_3CN.

	1 · 4CH_2Cl_2	**2** · 2.5$C_2H_4Cl_2$ · H_2O	**3** · 3DMF	**4** · 4CH_3CN
Empirical formula	$C_{60}H_{60}Cl_4O_8P_4Pt_2$ · 4CH_2Cl_2	$C_{60}H_{60}Cl_4Ni_2O_8P_4$ · 2.5$C_2H_4Cl_2$ · H_2O	$C_{59}H_{57}Cl_3Ni_2O_8P_4$ · 3DMF	$C_{58}H_{54}Cl_2Ni_2O_8P_4$ · 4CH_3CN
Formula weight	1904.63	1557.58	1460.99	1355.43
Crystal shape	prism	rod	needle	needle
Crystal dimensions (mm)	0.25 × 0.15 × 0.025	0.3 × 0.1 × 0.05	0.25 × 0.2 × 0.1	0.25 × 0.1 × 0.05
Colour	colourless	red	red	red
Crystal system	triclinic	monoclinic	triclinic	monoclinic
Space group	$P\bar{1}$	$P2(1)/n$	$P\bar{1}$	$P2(1)/c$
a (Å)	14.2262(3)	12.2978(4)	12.2709(1)	16.4460(2)
b (Å)	15.3145(3)	12.2633(3)	12.8065(2)	17.6790(2)
c (Å)	18.0654(4)	46.560(2)	23.1120(3)	23.4653(3)
α (°)	89.674(1)		79.2779(7)	
β (°)	81.425(1)	91.024(1)	85.8389(8)	110.5541(7)
γ (°)	73.415(1)		77.1085(8)	
V (Å^3)	3727.1(1)	7020.7(4)	3476.80(8)	6388.2(1)
T (K)	293	243	243	243
Z	2	4	2	4
D_{calc} (Mg/m^3)	1.697	1.474	1.389	1.406
Absorption coefficient (mm^{-1})	4.315	1.024	0.809	0.831
F(000)	1872	3204	1510	2804
θ range for data collection (°)	1.51–26.41	2.13–25.12	1.79–27.55	1.48–26.04
Limiting indices	$-14 \leqslant h \leqslant 17$	$-14 \leqslant h \leqslant 14$	$-15 \leqslant h \leqslant 15$	$-20 \leqslant h \leqslant 20$
	$-19 \leqslant k \leqslant 19$	$-14 \leqslant k \leqslant 14$	$-16 \leqslant k \leqslant 16$	$-21 \leqslant k \leqslant 21$
	$-22 \leqslant l \leqslant 22$	$-55 \leqslant l \leqslant 55$	$-30 \leqslant l \leqslant 30$	$-28 \leqslant l \leqslant 25$
Reflections collected	24853	13622	30555	42124
Independent reflections (R_{int})	15307 (0.0426)	12550 (0.0420)	15883 (0.0414)	12598 (0.0377)
Absorption correction	multi-scan			
Refinement method	full-matrix least-squares on F^2			
Data/restraints/parameters	14963/0/811	8506/2/829	15883/0/835	12598/5/780
Goodness-of-fit on F^2	1.037	1.030	1.037	1.033
Final *R* indices [$I > 2\sigma(I)$, **1**, **3**, **4**; $I > 3\sigma(I)$, **2**]	R_1 = 0.0311, wR_2 = 0.0807	R_1 = 0.0510, wR_2 = 0.1238	R_1 = 0.0379, wR_2 = 0.1085	R_1 = 0.0347, wR_2 = 0.0909
R indices (all data)	R_1 = 0.0414, wR_2 = 0.0984	R_1 = 0.0691, wR_2 = 0.1644	R_1 = 0.0530, wR_2 = 0.1371	R_1 = 0.0465, wR_2 = 0.1093
Largest difference in peak and hole (e Å^{-3})	0.810 and −0.680	0.620 and −0.470	0.650 and −0.360	0.340 and −0.350

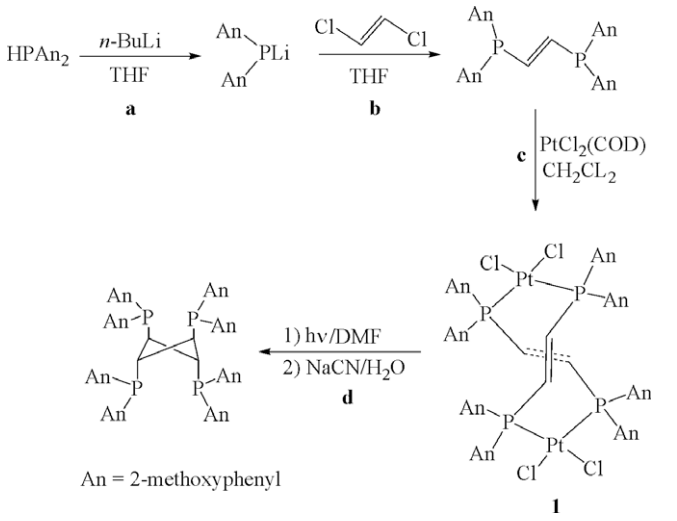

Scheme 2.

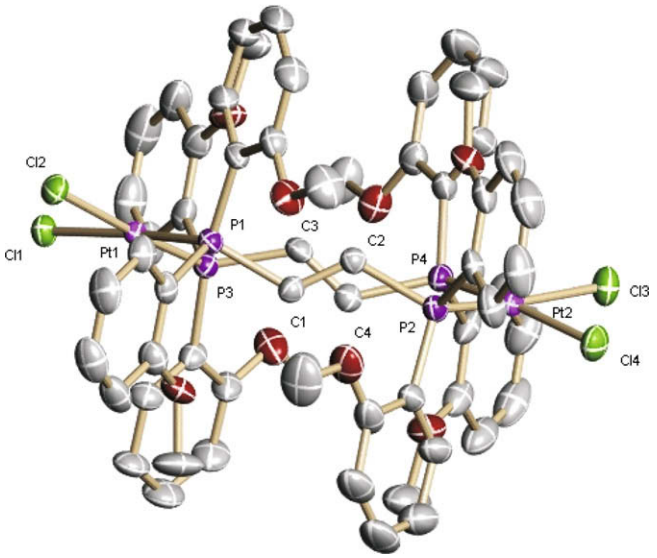

Fig. 1. ORTEP diagram of **1** · $4CH_2Cl_2$. Hydrogen atoms and solvent molecules are omitted for clarity and thermal ellipsoids are shown at the 30% probability level.

configuration in *o*-MeO-dppcb has been provided so far due to the fact that **1** is extremely difficult to crystallize and highly air sensitive single crystals loosing CH_2Cl_2 within seconds can only be obtained retrosynthetically. In this regard, we report here the synthesis (Scheme 2, step c) and full characterization of **1**, that represents the key compound in the synthesis of *o*-MeO-dppcb (Scheme 2, steps a–d).

The reaction of *trans*-*o*-MeO-dppen with [$PtCl_2(\eta^4$-COD)] in a 1:1 molar ratio selectively yielded the dinuclear *trans*-*o*-MeO-dppen bridged compound [Pt_2Cl_4(μ-(κP^1:κP^2-*o*-MeO-*trans*-dppen))$_2$] (**1**), that has been isolated with 92.2% yield. The $^{31}P\{^1H\}$ NMR spectrum of the latter compound, acquired in CD_2Cl_2, exhibited one singlet centered at −5.9 ppm and a $^1J_{PtP}$ parameter of 3640 Hz, that is comparable to the corresponding value of 3550 Hz found for the phenyl-counterpart [Pt_2Cl_4(μ-(κP^1:κP^2-*trans*-dppen))$_2$] [15].

Compound **1** has been characterized by multinuclear NMR spectroscopy, mass spectrometry (FAB, using 3-nitrobenzylalcohol as matrix), elemental analysis, and by a single crystal X-ray structure analysis (*vide infra*). An ORTEP plot of **1** · $4CH_2Cl_2$ is presented in Fig. 1, while crystallographic data and selected bond distances and angles are shown in Tables 1 and 2, respectively.

The crystal structure of **1** · $4CH_2Cl_2$ contains four molecules of CH_2Cl_2 per asymmetric unit. Both metal centers show a square-planar coordination sphere that is built up by two *cis*-coordinating phosphorus donor atoms of two different bridging phosphane ligands. The coordination sphere of both metal centers is completed by two chloride atoms. Both P–Pt–P coordination angles of 99.94(5)° and 100.56(6)° (Table 2) are significantly larger when compared to that observed for the related complex [Pt_2Cl_4(μ-(κP^1:κP^2-*trans*-dppen))$_2$] of 94.77(14)° and 95.08(14)° [15]. The most striking structural difference between the latter compound and **1** · $4CH_2Cl_2$ is the relative orientation of the adjacent C=C double bonds of the coordinating *trans*-*o*-MeO-dppen ligands in the dinuclear complexes. This has a crucial effect on the outcome of the photochemically induced [2+2] cycloaddition reaction. In this regard, a Newman projection along the carbon atoms C(1) and C(3) in **1** · $4CH_2Cl_2$ (Fig. 1) shows a dihedral angle of 68.1(4)°, whereas the analogous projection for the phenyl-counterpart [Pt_2Cl_4(μ-(κP^1:κP^2-*trans*-dppen))$_2$] exhibited only a value of 34.8° [15]. This significant difference in the relative orientation of the C=C double bonds to each other in both latter Pt-complexes selectively leads to an all-*trans* orientation of the phosphanyl groups in *o*-MeO-dppcb (see Scheme 2). By contrast, [Pt_2Cl_4(μ-(κP^1:κP^2-*trans*-dppen))$_2$] produces a *cis,trans,cis* orientation of the phosphanyl groups in dppcb, where dppcb is *cis,trans,cis*-1,2,3,4-tetrakis(diphenylphosphanyl)cyclobutane [15]. Since [2+2] cycloaddition reactions where both reacting C=C double bonds are perpendicular to each other are photochemically forbidden, according to the Woodward and Hoffmann rules of orbital symmetry [16,17], we are not in the condition to either confirm or rule out a radical mechanism that might be operative in the intramolecular formation of the cyclobutane carbon ring of *o*-MeO-dppcb. A similar situation has been found to occur for the synthesis of 1,2-bis(diphenylphosphanyl)-3,4-diphenylcyclobutane [18].

Table 2
Selected bond lengths (Å) and bond angles (°) for **1** · $4CH_2Cl_2$.

Bond lengths (Å)		Bond angles (°)	
Pt(1)–P(1)	2.2498(15)	P(1)–Pt(1)–P(3)	99.94(5)
Pt(1)–P(3)	2.2458(16)	P(3)–Pt(1)–Cl(1)	87.03(6)
Pt(1)–Cl(1)	2.3470(16)	P(1)–Pt(1)–Cl(1)	171.58(5)
Pt(1)–Cl(2)	2.3597(17)	P(3)–Pt(1)–Cl(2)	172.41(5)
Pt(2)–P(2)	2.2430(16)	P(1)–Pt(1)–Cl(2)	86.14(6)
Pt(2)–P(4)	2.2476(15)	Cl(1)–Pt(1)–Cl(2)	87.31(6)
Pt(2)–Cl(3)	2.3444(17)	P(2)–Pt(2)–P(4)	100.56(6)
Pt(2)–Cl(4)	2.3514(16)	P(2)–Pt(2)–Cl(3)	169.30(6)
C(1)–C(2)	1.301(7)	P(4)–Pt(2)–Cl(3)	87.53(6)
C(3)–C(4)	1.309(7)	P(2)–Pt(2)–Cl(4)	85.57(6)
		P(4)–Pt(2)–Cl(4)	170.85(6)
		Cl(3)–Pt(2)–Cl(4)	87.28(6)

The relative all-*trans* configuration of the *o*-methoxyphenylphosphanyl groups with respect to the cyclobutane carbon ring in *o*-MeO-dppcb has been confirmed by several single crystal X-ray structure analyses of dimeric Pt(II) [11], Pd(II) [11] and Ni(II) complexes (*vide infra*). Though 1,2-bis(diphenylphosphanyl)-3,4-diphenylcyclobutane also shows an all-*trans* arrangement [18], to the best of our knowledge *o*-MeO-dppcb is the first example of a cyclobutane derivative with four phosphorus substituents in this all-*trans* configuration. Unlike the *cis,trans,cis* orientation of the diphenylphosphanyl substituents in dppcb [19], the all-*trans* configuration of the substituted phosphanyl groups in *o*-MeO-dppcb implies two possible coordination modes of the ligand, that comprise an 1,2-*cis*, or 1,3-*cis* coordination of the phosphorus donor atoms to the same metal center. As a result, either two five-mem-

bered or two six-membered metallacycles are obtained (Scheme 3) [11].

3.2. Single crystal X-ray structure of [Ni_2Cl_4(μ-(κP^1:κP^2:κP^3:κP^4-*o*-MeO-dppcb)] (**2**) and its stepwise methoxy-group cleavage

Unlike the reaction of *o*-MeO-dppcb with Pt(II) and Pd(II), the reaction with $NiCl_2 \cdot 6H_2O$ selectively yielded the dimeric complex **2**, that is characterized by two six-membered metallacycles sharing a folded cyclobutane carbon ring, as shown in the ORTEP plot of the single crystal X-ray structure of **2** $\cdot$ $2.5C_2H_4Cl_2 \cdot H_2O$ (Fig. 2).

The crystal structure of compound **2** $\cdot$ $2.5C_2H_4Cl_2 \cdot H_2O$ shows for both Ni(II) centers square pyramidal coordination spheres. While the basal coordination sites are occupied by two 1,3-*cis*-coordinating phosphorus donor atoms of *o*-MeO-dppcb (Scheme 3) and two chloride atoms, the apical coordination sites are occupied by methoxy-oxygen atoms of the ligand (Ni(1)–O(6) 2.604(6) Å, Ni(2)–O(3) 2.621(5) Å, Fig. 2 and Table 3). As a result, the two phosphorus donor atoms coordinating to the same Ni(II) center are not equivalent, showing at least at Ni(2) significantly

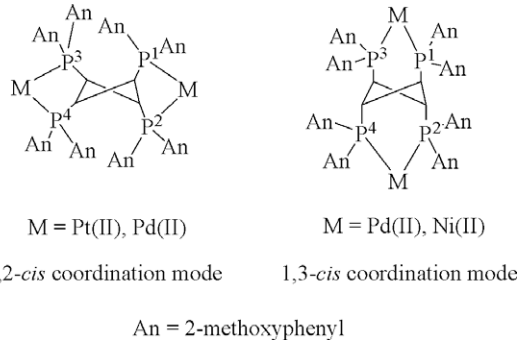

Scheme 3.

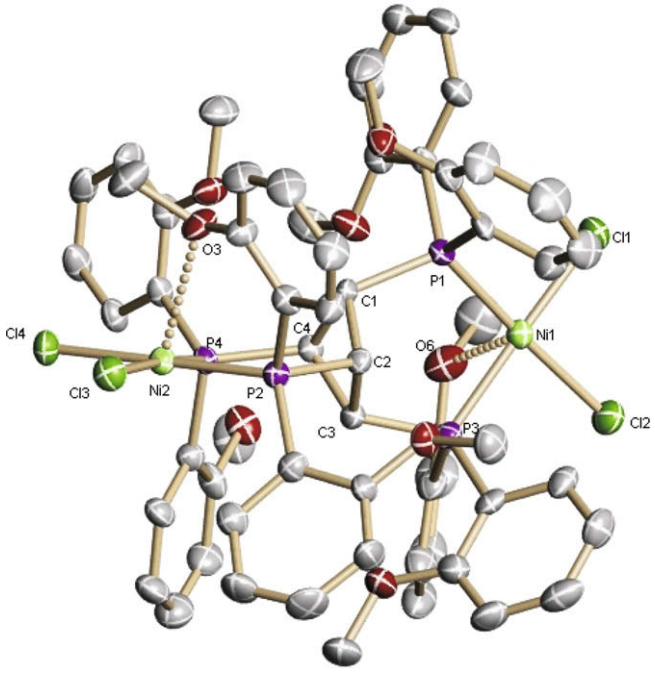

Fig. 2. ORTEP diagram of **2** $\cdot$ $2.5C_2H_4Cl_2 \cdot H_2O$. Hydrogen atoms and solvent molecules are omitted for clarity and thermal ellipsoids are shown at the 30% probability level.

different Ni–P distances of 2.186(2) and 2.174(2) Å (Table 3), while the P–Ni–P bite angles of 94.86(7)° (P(1)–Ni(1)–P(3)) and 95.01(8)° (P(2)–Ni(2)–P(4)) are identical within statistical significance.

It is important to emphasize at this point, that the inequivalence of the phosphorus donor atoms observed in the solid state persists also in solution. Accordingly, the $^{31}P\{^1H\}$ NMR spectrum of **2** showed at room temperature two doublets at 7.37 and 25.55 ppm ($^2J_{PP}$ = 94.0 Hz), while the ^1H NMR spectrum exhibited two broad down-field shifted singlets centered at 9.60 and 10.48 ppm, evidencing Ni(II) *ortho*-methoxy-oxygen interactions that occur in solution [11]. Similar metal–oxygen interactions have been also observed in other complexes containing *ortho*-methoxy-modified phosphanes [11,20].

Intrigued by the fact that two methoxy-oxygen atoms are very close to both Ni(II) centers in **2** $\cdot$ $2.5C_2H_4Cl_2 \cdot H_2O$, we studied the thermal behavior of **2** in solution in order to gain information on a possible intramolecular methoxy C–O cleavage, obtaining thus a phenolate moiety, that coordinates to Ni(II). For this purpose, a variable-temperature $^{31}P\{^1H\}$ NMR spectroscopic study was carried out with **2** dissolved in DMF-d^7 and a sequence of selected $^{31}P\{^1H\}$ NMR spectra of this study are shown in Fig. 3.

The $^{31}P\{^1H\}$ NMR spectrum of a deaerated solution of **2** in DMF-d^7 showed two doublets centered at 6.50 and 24.80 ppm ($^2J_{PP}$ = 94.0 Hz (Fig. 3, trace a)). This latter NMR solution was then gradually heated from room temperature to 80 °C (Fig. 3, trace b) at a temperature interval of 10 °C. Since $^{31}P\{^1H\}$ NMR spectra acquired at temperatures higher than 40 °C showed no signal, the NMR probe always has been cooled back to room temperature, followed by the acquisition of a $^{31}P\{^1H\}$ NMR spectrum, before it has been heated to a temperature that was 10 °C higher compared to the previous one. From this heating and cooling sequence of the DMF-d^7 solution of **2** turned out that the latter compound was converted into the unsymmetrical mono-phenolate complex of the formula [Ni_2Cl_3(μ-(κO^1,κP^1:κP^2:κP^3:κP^4-*o*-MeO-*O*-dppcb))] (**3**) (Scheme 4) at 80 °C in a time interval of 1.5 h.

Accordingly, the $^{31}P\{^1H\}$ NMR spectrum showed for **3** four broad humps centered at 7.80, 20.70, 28.10 and 36.10 ppm (Fig. 3, trace c), due to the asymmetry of the molecule and in accordance with a fluxional structure. However, in contrast to [Ni_2Cl_2(μ-(κO^1,κP^1:κP^2:κO^2,κP^3:κP^4-*o*-MeO-*o*-*O*,*O*′-dppcb)] (**4**) this fluxional behavior could not be resolved by cooling the NMR solution to −90 °C (*vide infra*). The $^{31}P\{^1H\}$ NMR signal at 36.10 ppm has been assigned to the phosphorus atom bearing the phenolate moiety. After the conversion of **2** into **3** had been completed, the NMR solution was heated to 100 °C. The first $^{31}P\{^1H\}$ NMR spectrum at that temperature showed the occurrence of two broad humps centered at 23.10 and 38.80 ppm (Fig. 3, trace d). Prolonged heating (i.e. for 1.5 h) of the NMR solution at this latter temperature brought about the complete conversion of **3** into the bis-phenolate complex of the formula [Ni_2Cl_2(μ-(κO^1,κP^1:κP^2:κO^2,κP^3:κP^4-*o*-MeO-*o*-*O*,*O*′-dppcb)] (**4**) (Scheme 4 and Fig. 3, trace e). A successively acquired $^{31}P\{^1H\}$ NMR spectrum at room temperature confirmed the quantitative conversion of **3** into **4** (Fig. 3, trace f). In accordance with the symmetric structure of **4**, the $^{31}P\{^1H\}$ NMR spectrum shows a multiplet at 22.80 and a hump at 39.90 ppm, that have been assigned to the couple of achiral and chiral phosphorus atoms, respectively.

In the light of the experimental results obtained from the variable-temperature NMR experiment of **2**, compounds **3** and **4** have been synthesized independently, following a synthetic protocol as shown in Scheme 4. The isolated compounds **3** and **4** were obtained as micro-crystalline powders with 61.8% and 95.9% yield, respectively. Both latter complexes have been characterized by multinuclear NMR spectroscopy, mass spectrometry (FAB, using 3-nitrobenzylalcohol as matrix), elemental analyses, and by single crystal X-ray structure analyses (*vide infra*).

Table 3
Selected bond lengths (Å) and bond angles (°) for **2** · $2.5C_2H_4Cl_2 \cdot H_2O$, **3** · 3DMF and **4** · $4CH_3CN$.

Bond lengths (Å)				Bond angles (°)			
	2	**3**	**4**		**2**	**3**	**4**
Ni(1)–P(1)	2.182(2)	2.1691(11)	2.1477(9)	P(1)–Ni(1)–P(3)	94.86(7)	95.00(4)	94.59(4)
Ni(1)–P(3)	2.182(2)	2.1783(10)	2.1291(10)	P(1)–Ni(1)–Cl(1)	86.46(8)	177.12(3)	90.28(4)
Ni(1)–Cl(1)	2.206(2)	2.2005(12)	2.1993(9)	P(1)–Ni(1)–Cl(2)	173.73(10)	86.14(4)	
Ni(1)–Cl(2)	2.244(2)	2.2058(10)		P(3)–Ni(1)–Cl(1)	178.68(9)	87.87(4)	170.71(3)
Ni(1)–O(1)	3.787(6)	3.517(2)	5.098(2)	P(3)–Ni(1)–Cl(2)	86.55(8)	178.12(3)	
Ni(1)–O(2)	5.169(5)	5.095(3)	3.226(2)	Cl(1)–Ni(1)–Cl(2)	92.15(8)	90.98(4)	
Ni(1)–O(5)	5.194(5)	5.176(2)	5.004(3)	P(1)–Ni(1)–O(6)			169.77(7)
Ni(1)–O(6)	2.604(6)	3.340(2)	1.891(2)	P(3)–Ni(1)–O(6)			84.44(7)
Ni(2)–P(2)	2.186(2)	2.1217(9)	2.1313(10)	O(6)–Ni(1)–Cl(1)			92.14(7)
Ni(2)–P(4)	2.174(2)	2.1578(9)	2.1585(10)	P(2)–Ni(2)–P(4)	95.01(8)	92.07(4)	91.95(3)
Ni(2)–Cl(3)	2.226(2)	2.2045(10)		P(2)–Ni(2)–Cl(2)			168.82(4)
Ni(2)–Cl(4)	2.208(2)			P(2)–Ni(2)–Cl(3)	88.42(8)	164.12(4)	
Ni(2)–Cl(2)			2.1953(10)	P(2)–Ni(2)–Cl(4)	179.66(9)		
Ni(2)–O(3)	2.621(5)	1.906(2)	1.905(2)	P(2)–Ni(2)–O(3)		87.02(7)	86.52(7)
Ni(2)–O(4)	5.221(5)	2.949(2)	2.861(2)	P(4)–Ni(2)–Cl(2)			92.86(4)
Ni(2)–O(7)	5.136(5)	5.155(3)	5.144(2)	P(4)–Ni(2)–Cl(3)	173.35(9)	92.17(4)	
Ni(2)–O(8)	3.583(5)	3.470(3)	3.275(3)	P(4)–Ni(2)–Cl(4)	85.26(8)		
				P(4)–Ni(2)–O(3)		162.46(8)	164.43(8)
				Cl(4)–Ni(2)–Cl(3)	91.29(8)		
				Cl(3)–Ni(2)–O(3)		93.45(8)	
				O(3)–Ni(2)–Cl(2)			91.50(7)

The $^{31}P\{^1H\}$ NMR spectrum of the independently synthesized compound **3**, acquired in CD_2Cl_2, showed analogously to that acquired in DMF-d^7 (Fig. 3, trace c) four broad humps centered at 9.43, 21.80, 29.25 and 36.70 (i.e. chiral phosphorus) ppm, while the corresponding ^1H NMR spectrum exhibited for the methoxy-group hydrogen atoms very broad and poorly resolved singlets in the chemical shift range from 2.60 to 3.62 ppm, indicating a completely asymmetric molecule. A FAB-spectrum of the latter compound showed a peak at *m*/*z* of 1205.5 that has been assigned to the $[M-Cl]^+$ fragment.

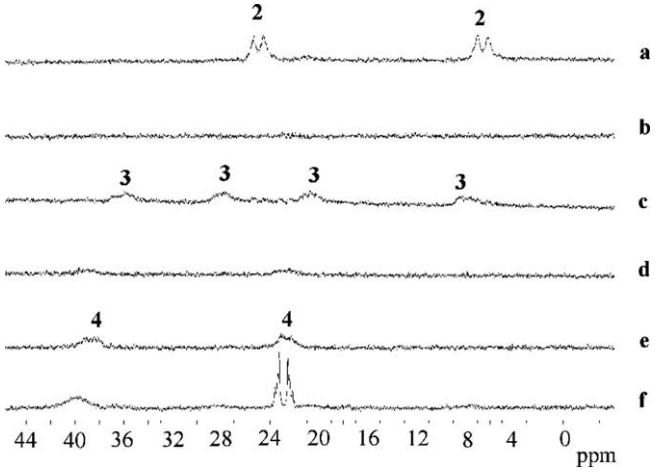

Fig. 3. Variable-temperature $^{31}P\{^1H\}$ NMR study of **2** (DMF-d^7, 121.50 MHz): (a) under nitrogen at room temperature; (b) after heating the NMR solution to 80 °C; (c) after cooling the NMR solution (1.5 h at 80 °C) to room temperature; (d) after heating the NMR solution to 100 °C; (e) after heating the NMR solution at 100 °C for 1.5 h and (f) after cooling the NMR solution to room temperature.

The $^{31}P\{^1H\}$ NMR spectrum of compound **4**, acquired in CD_2Cl_2, exhibited at room temperature a broad hump centered at 39.50 ppm and a multiplet of higher order centered at 23.30 ppm. Upon cooling the latter NMR solution to −80 °C, the hump in the $^{31}P\{^1H\}$ spectrum at 39.50 ppm, that has been assigned to the couple of chiral phosphorus atoms, has been resolved very nicely into a multiplet, while the multiplet at 23.30 ppm only experienced a slight shift upon cooling the NMR solution. Since the $^{31}P\{^1H\}$ NMR spectrum of **4** is of higher order, it has been successfully simulated employing the following NMR parameters: $\delta^1 = 41.39$, $\delta^2 = 41.45$, $\delta^3 = \delta^4 = 23.98$ ppm, $^2J_{PP} = 83.0$ Hz and $^3J_{PP} = 29.0$ Hz [12].

*3.3. Single crystal X-ray structures of [Ni_2Cl_3(μ-(κO^1,κP^1:κP^2:κP^3:κP^4-o-MeO-o-O-dppcb))] (**3**) and [Ni_2Cl_2(μ-(κO^1,κP^1:κP^2:κO^2,κP^3:κP^4-o-MeO-o-O,O′-dppcb)] (**4**)*

A single crystal X-ray structure analysis of **3** · 3DMF unambiguously confirmed the occurrence of a phosphanylphenolate ligand bearing one coordinating phenolate unit bonded to a chiral phos-

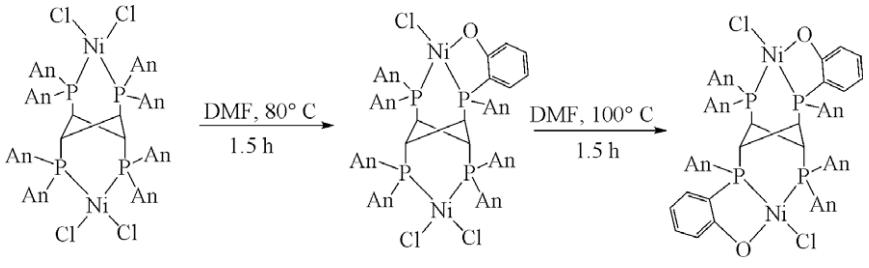

Scheme 4.

phorus donor atom. As a result the ligand acts as a bridging κ^2-*P,P* and κ^3-*P,P,O* ligand. An ORTEP drawing of the molecular structure is shown in Fig. 4, while selected bond distances and angles are reported in Table 3.

The crystal structure of compound **3** · 3DMF shows for both Ni(II) centers two different square-planar coordination spheres. While Ni(1) is 1,3-*cis* coordinated by two phosphorus donor atoms (see Scheme 3) and two chloride atoms, Ni(2) binds to two 2,4-*cis*-coordinating phosphorus atoms, to one chloride atom, and to a phenolate oxygen atom. As a consequence, one of the phosphorus atoms (i.e. P(2)) that bears the phenolate unit and the cyclobutane carbon atom C(2) (see Fig. 4) constitutes a center of chirality. The coordination of the phenolate oxygen atom O(3) to Ni(2) leads to a completely asymmetric molecule that is clearly evidenced by four different Ni–P distances ranging from 2.1217(9) Å for Ni(2)–P(2) to 2.1783(10) Å for Ni(1)–P(3) (see Table 3). In accordance with this, also the P–Ni–P bite angles are significantly different, showing for P(1)–Ni(1)–P(3) 95.00(4)° and for P(2)–Ni(2)–P(4) 92.07(4)°. A further consequence of the phenolate coordination to Ni(2) is that unlike **2** · $2.5C_2H_4Cl_2$ · H_2O, **3** · 3DMF shows no significant methoxy-oxygen interactions at Ni(1) (see Table 3), due to a slight conformational change of the ligand upon the coordination of the phenolate unit to Ni(2). As a consequence, the energy barrier for the second methoxy-cleavage that occurred at Ni(1) has to be significantly higher compared to the first one. Accordingly, the variable-temperature $^{31}P\{^1H\}$ NMR experiment showed that the conversion of **3** into **4** occurs at a temperature that is 20 °C higher compared to that found for the conversion of **2** into **3** (i.e. 100 versus 80 °C) (Fig. 3).

A single crystal structure analysis of compound **4** · $4CH_3CN$ (Fig. 5) confirmed the occurred double methoxy-group cleavage and the formation of a symmetrical κ^3-*P,P,O*-coordinating bis-phenolate ligand, leading to one coordinating phenolate unit at each metal center (see Scheme 4 and Fig. 5).

The crystal structure of **4** · $4CH_3CN$ shows for both Ni(II) centers a square-planar coordination geometry with two 1,3-*cis*-coordinating phosphorus atoms (see Scheme 3), a phenolate oxygen atom and a chloride atom. Due to the presence of two phenolate moieties attached to phosphorus atoms that belong to different Ni-coordination spheres, in **4** · $4CH_3CN$ two phosphorus atoms (i.e. P(2) and P(3)) and the cyclobutane carbon atoms represent centers of chirality. Additionally, the latter compound exhibits a chiral axis due to the rigid folding of the cyclobutane ring that is perpendicular to the best plane defined by the cyclobutane carbon atoms. However, since only one pair of diastereomers is formed, these centers of chirality are obviously related to each other as a consequence of seven fused rings (see Fig. 5). All Ni–P bonding distances in **4** · $4CH_3CN$ are significantly shorter compared to those observed in **2** · $2.5C_2H_4Cl_2$ · H_2O (Table 3). Like **3** · 3DMF, **4** · $4CH_3CN$ shows significantly shorter Ni–P bonds for the chiral phosphorus atoms (i.e. P(2) and P(3), Fig. 5), due to the fact that the latter atoms share two five- and six-membered metallacycles, respectively. Importantly, the two coordination moieties of **4** · $4CH_3CN$ are not identical, clearly evidenced by the significantly different P–Ni–P bite angles of 94.59(4)° and 91.95(3)°.

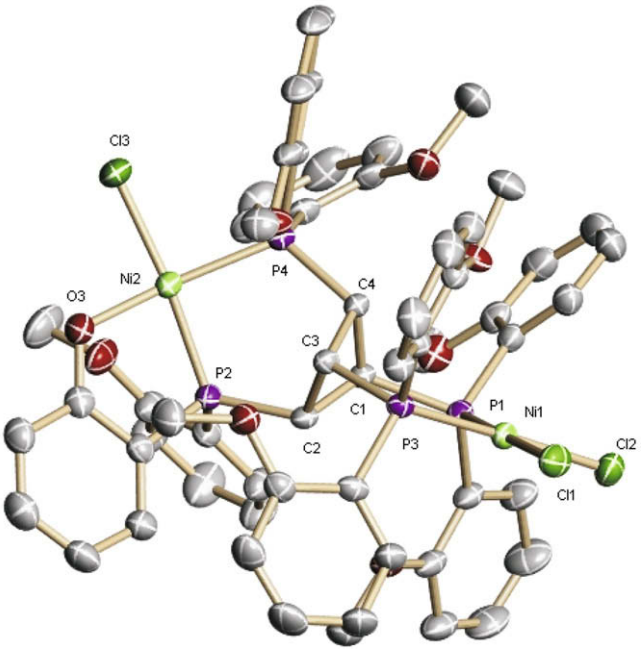

Fig. 4. ORTEP diagram of **3** · 3DMF. Hydrogen atoms and solvent molecules are omitted for clarity and thermal ellipsoids are shown at the 30% probability level.

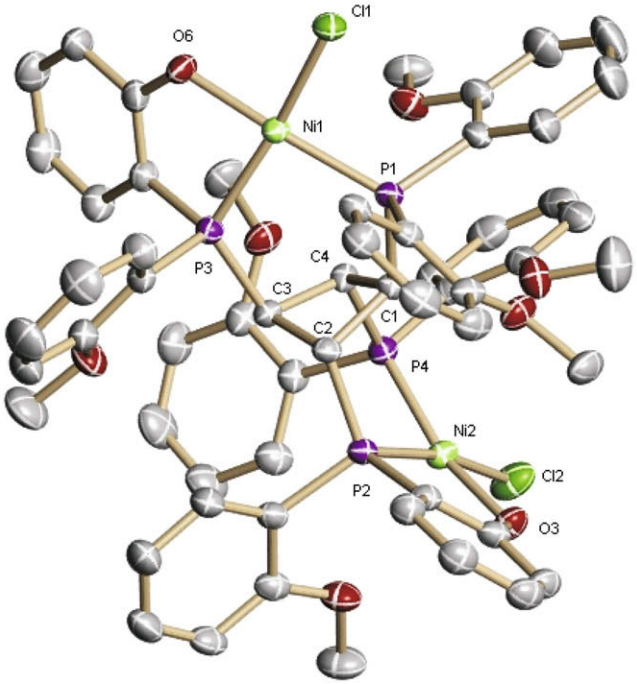

Fig. 5. ORTEP diagram of **4** · $4CH_3CN$. Hydrogen atoms and solvent molecules are omitted for clarity and thermal ellipsoids are shown at the 30% probability level.

4. Conclusions

The dinuclear Pt-complex (**1**) that represents the key compound in the synthesis of *o*-MeO-dppcb by an intramolecular [2+2] photocycloaddition, exploiting the template effect of **1**, has been synthesized and completely characterized. The single crystal X-ray structure analysis of the latter complex gives a convincing clue for the selective formation of the all-*trans* configuration regarding the bis(*o*-methoxyphenylphosphanyl) groups attached to the cyclobutane carbon ring in *o*-MeO-dppcb. Obviously, π-stacking interactions between adjacent *o*-methoxyphenyl groups in **1** that are clearly visible in Fig. 1, occur as a consequence of "steric pressure" [21]. Thus, the orientations of the bridges in **1** change due to this "steric pressure", compared with the phenyl-counterpart $[Pt_2Cl_4(\mu\text{-}(\kappa P^1{:}\kappa P^2\text{-}trans\text{-dppen}))_2]$, where no analogous π-stacking interactions between adjacent phenyl groups are present [15].

The single crystal structure analysis of the dinuclear Ni(II) complex **2** that contains all-*trans*-*o*-MeO-dppcb in the 1,3-*cis*-coordinating mode (Scheme 3), exhibits one Ni(II)–*o*-MeO–oxygen

interaction in both coordination spheres. These latter interactions have been exploited to convert **2**, upon a thermal reaction, first into the mono-phenolate complex **3** and then into the bis-phenolate complex **4**. This intramolecular methoxy-group cleavage occurring step by step is due to a slight conformational change of the ligand *o*-MeO-*O*-dppcb, as a consequence of the κ^2-*P*,*P* and κ^3-*P*,*P*,*O*-coordination modes of this ligand to the Ni(II) centers. Compounds **3** and **4** have been isolated and fully characterized in solution and in the solid state. Their single crystal X-ray diffraction analyses have been reported and discussed.

Attempts to de-coordinate and isolate the new phosphanophenolate ligands *o*-MeO-*O*-dppcb and *o*-MeO-*O*,*O*′-dppcb from **3** and **4**, respectively, are in progress in our laboratory.

Acknowledgments

The authors thank the Fonds zur Förderung der wissenschaftlichen Forschung (FWF) and the Forschungsförderungsgesellschaft (FFG), Vienna, Austria, the Tiroler Wissenschaftsfonds, Innsbruck, Austria, and the companies D. Swarovski and Co. and VERBUND – Austrian Renewable Power GmbH for financial support.

Appendix A. Supplementary material

CCDC 710161, 710162, 710163 and 710164 contain the supplementary crystallographic data for this paper. These data can be obtained free of charge from The Cambridge Crystallographic Data Centre via www.ccdc.cam.ac.uk/data_request/cif. Supplementary data associated with this article can be found, in the online version, at doi:10.1016/j.ica.2009.03.009.

References

[1] (a) P. Kuhn, D. Sémeril, D. Matt, M.J. Chetcuti, P. Lutz, Dalton Trans. (2007) 515;
(b) W. Keim, F.H. Kowaldt, R. Goddard, C. Krüger, Angew. Chem., Int. Ed. Engl. 17 (1978) 466;
(c) V. Gibson, A. Tomov, A.J.P. White, D.J. Williams, Chem. Commun. (2001) 719;
(d) J. Pietsch, P. Braunstein, Y. Chauvin, New J. Chem. (1998) 467;
(e) M. Bonnet, F. Dahan, A. Ecke, W. Keim, R.P. Schulz, I. Tkatchenko, J. Chem. Soc., Chem. Commun. (1994) 615;
(f) W. Keim, R.P. Schulz, J. Mol. Catal. 92 (1994) 21;
(g) F.M. Bauer, S. Mecking, Macromolecules 34 (2001) 1165;
(h) R. Soula, J.P. Broyer, M.F. Llauro, A. Tomov, R. Spitz, J. Claverie, X. Drujon, J. Malinge, T. Saudemont, Macromolecules 34 (2001) 2438.
[2] J. Heinicke, R. Kadyrov, M.K. Kindermann, M. Koesling, P.G. Jones, Chem. Ber. 129 (1996) 1547.
[3] J. Heinicke, R. Kadyrov, J. Organomet. Chem. 520 (1996) 131.
[4] J. Heinicke, M. Köhler, N. Peulecke, M. He, M.K. Kindermann, W. Keim, G. Fink, Chem. Eur. J. 9 (2003) 6093.
[5] M.K. Cooper, J.M. Downes, P.A. Duckworth, E.R.T. Tiekink, Austr. J. Chem. 45 (1992) 595.
[6] J.A. Van Doorn, N.K. Meijboom, Recl. Trav. Chim. Pays-Bas 111 (1992) 170.
[7] J. Heinicke, N. Peulecke, M.K. Kindermann, P.G. Jones, Z. Anorg. Allg. Chem. 631 (2005) 67.
[8] (a) T. Imamoto, K. Yashio, K.V.L. Crépy, K. Katagiri, H. Takahashi, M. Kouchi, I.D. Gridnev, Organometallics 25 (2006) 908;
(b) S. Chatterjee, R. Doyle, D.C.R. Hockless, G. Salem, A.C. Willis, Dalton Trans. (2000) 1829.
[9] R.C. van der Drift, E. Bouwman, E. Drent, H. Kooijman, A.L. Spek, A.B. van Oort, W.P. Mul, Organometallics 21 (2002) 3401.
[10] C. Bianchini, G. Lenoble, W. Oberhauser, S. Parisel, F. Zanobini, Eur. J. Inorg. Chem. (2005) 4794.
[11] M. Fessler, S. Eller, B. Trettenbrein, G. Czermak, P. Brüggeller, L. Bettucci, C. Bianchini, A. Meli, A. Ienco, W. Oberhauser, Dalton Trans. (2009) 1859.
[12] M. Probst, INSIM-GUI V 1.0, A Computer Program for NMR Simulation, University of Innsbruck, Innsbruck, Austria, 1998.
[13] Z. Otwinowski, W. Minor, in: C.W. Carter Jr., R.M. Sweet (Eds.), Methods in Enzymology, Macromolecular Crystallography, Part A, vol. 276, Academic Press, New York, 1997, p. 307.
[14] G.M. Sheldrick, SHELXL-97, A Computer Program for Crystal Structure Determination, University of Göttingen, Göttingen, Germany, 1997.
[15] W. Oberhauser, C. Bachmann, T. Stampfl, R. Haid, C. Langes, H. Kopacka, A. Rieder, P. Brüggeller, Inorg. Chim. Acta 290 (1999) 167.
[16] R.B. Woodward, R. Hoffmann, Angew. Chem. 81 (1969) 797.
[17] R.B. Woodward, R. Hoffmann, Angew. Chem., Int. Ed. Engl. 8 (1969) 781.
[18] W.-C. Yeo, G-K. Tan, L.L. Koh, P.-H. Leung, Eur. J. Inorg. Chem. (2005) 4723.
[19] C. Bianchini, L. Gonsalvi, W. Oberhauser, D. Sémeril, P. Brüggeller, Dalton Trans. (2003) 3869.
[20] (a) I.M. Angulo, E. Bouwman, S.M. Lok, M. Lutz, W.P. Mul, A.L. Spek, Eur. J. Inorg. Chem. (2001) 1465;
(b) C. Bianchini, A. Meli, W. Oberhauser, A.M. Segarra, C. Claver, E.J. Garcia Suarez, J. Mol. Catal. A: Chem. 265 (2007) 292;
(c) C. Bianchini, A. Meli, W. Oberhauser, C. Claver, E.J. Garcia Suarez, Eur. J. Inorg. Chem. (2007) 2702.
[21] (a) C. Bachmann, R. Gutmann, G. Czermak, A. Dumfort, S. Eller, M. Fessler, H. Kopacka, K.-H. Ongania, P. Brüggeller, Eur. J. Inorg. Chem. (2007) 3227;
(b) H.A. Mayer, W.C. Kaska, Chem. Rev. 94 (1994) 1239.